THE JOURNAL OF PHYSICAL CHEMISTRY C
A JOURNAL OF THE AMERICAN CHEMICAL SOCIETY

pubs.acs.org/JPCC

Article

Solution Processable Deep-Blue OLEDs Based on Benzimidazole-TPA Conjugated through 9,9-Diethyl Fluorene (D-π-A) Luminophore with a Hybridized Local and Charge Transfer Excited State

Sandhya Rani Nayak, Jaipal Devesing Girase, Mangey Ram Nagar, Jwo-Huei Jou, and Sivakumar Vaidyanathan*

Cite This: *J. Phys. Chem. C* 2023, 127, 10291−10302

Read Online

ACCESS | Metrics & More | Article Recommendations | Supporting Information

ABSTRACT: Blue emitters with outstanding luminous performance must be synthesized for full-color organic light-emitting diode displays. The hybridized local and charge transfer (HLCT) is a remarkable excited state that combines the local and CT state to ensure a significant fluorescence quantum yield. The ambition of this study is to implement a subtle interpretation of photophysical and electroluminescence (EL) properties. To understand more about the geometry and orientations, the density functional theories were studied. Herein, we present a hybrid donor-π-acceptor blue-emitting fluorophore with a twisted geometry, in which triphenylamine (TPA) acts as a donor, 9,9 diethylfluorene acts as a spacer, and benzilimidazole acts as an acceptor. The EL spectra of the device are very similar to spectra of photoluminescence in the solution phase. Among all, the best performing 15 wt % MCFBI-fl-TPA-based OLED device illustrates a maximum luminance of 3290 cd/m^2. The device shows 8.2 lm W^{-1} of power efficiency, 7.9 cd A^{-1} of current efficiency, and 3.5% of high external quantum efficiency with (0.20, 0.23) of CIE coordinates of the device emitting blue color.

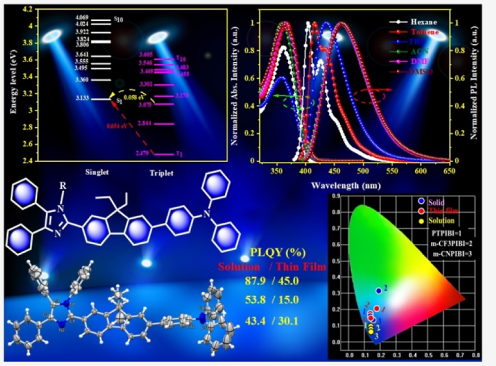

INTRODUCTION

In the era of lightning technology, huge passion in organic light-emitting diodes (OLEDs) have been extensively employed in different applications of full-color flat-panel display such as electrical gadgets (mobile phones, TVs, etc.).[1−10] An efficient emitter like deep-blue is widely recognized as critical in OLEDs, not only for the sake of harvest among three major colors (red, green, and blue) but also further due to the full visible region and white light generation via energy transfer. Due to the lack of efficient deep-blue emitters, commercialization of flat-panel displays and lighting is still limited. So far, the achievement of deep-blue OLEDs that fulfills the European Broadcasting Union's (EBU) standard index [chromaticity coordinates that is CIE of (0.15, 0.06)] requires significant development, as it remarkably approaches an external quantum efficiency (EQE) of 5% (highest limit of traditional fluorescent materials). As a result, developing high-performance deep-blue fluorophores is extremely important but also difficult, and much more research effort is required.[11,12]

In most of the luminescent materials, singlet excited states harvest 25% of excitons and triplet excited states harvest 75% of excitons. The 75% triplet excitons in typical materials of the fluorophores, on the other hand, are liable to dispersion due to thermal radiation. As a consequence, to use the 75% triplet exciton is crucial to increasing the material's exciton usage rate. Several methods adopted to harvest dark triplet exciton to ground state [such as, phosphorescent dopants, triplet−triplet annihilation (TTA), thermally activated delayed fluorescence (TADF), and HLCT] to boost the exciton utilizing efficiency in the device. TTA, TADF, and local charge-transfer electroluminescence (EL) are the three principal organic EL mechanisms that use triplet excitons thus far HLCT.[13−15] The more energy gap among lowest excited singlet state (S_1) and the lowest excited triplet state (T_1), the TTA prevails among the two triplet excitons and higher triplet state (T_m) with constant energy of singlet exciton (S_n) produces the upper convergence. Therefore, between T_m and S_n, the excitons of singlet state are generated by intersystem crossing (ISC) which subsequently increases the efficiency. In the ideal scenario, when the TTA process unfolds the theoretical highest limit ratio is still less than 62.5% of the singlet exciton comparing to an EQE of 12.5%.[16−18] It is difficult to harvest the exciton from T_1 to S_1 for efficient reverse intersystem crossing (RISC)

Received: February 4, 2023
Revised: May 2, 2023
Published: May 17, 2023

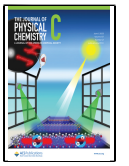

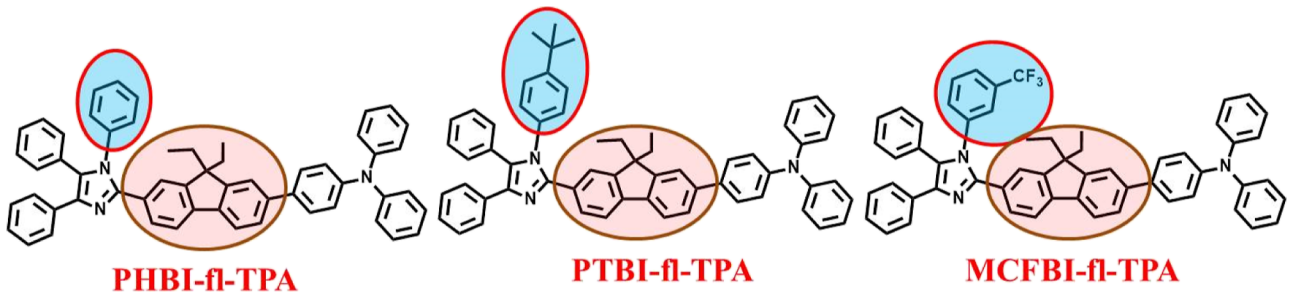

Figure 1. Molecular structure of BI-fl-TPA derivatives.

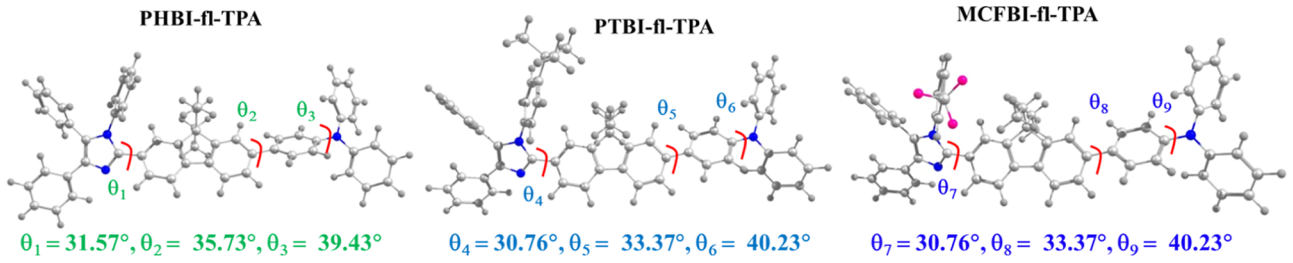

Figure 2. Optimized structure with dihedral angles of BI-fl-TPA derivatives.

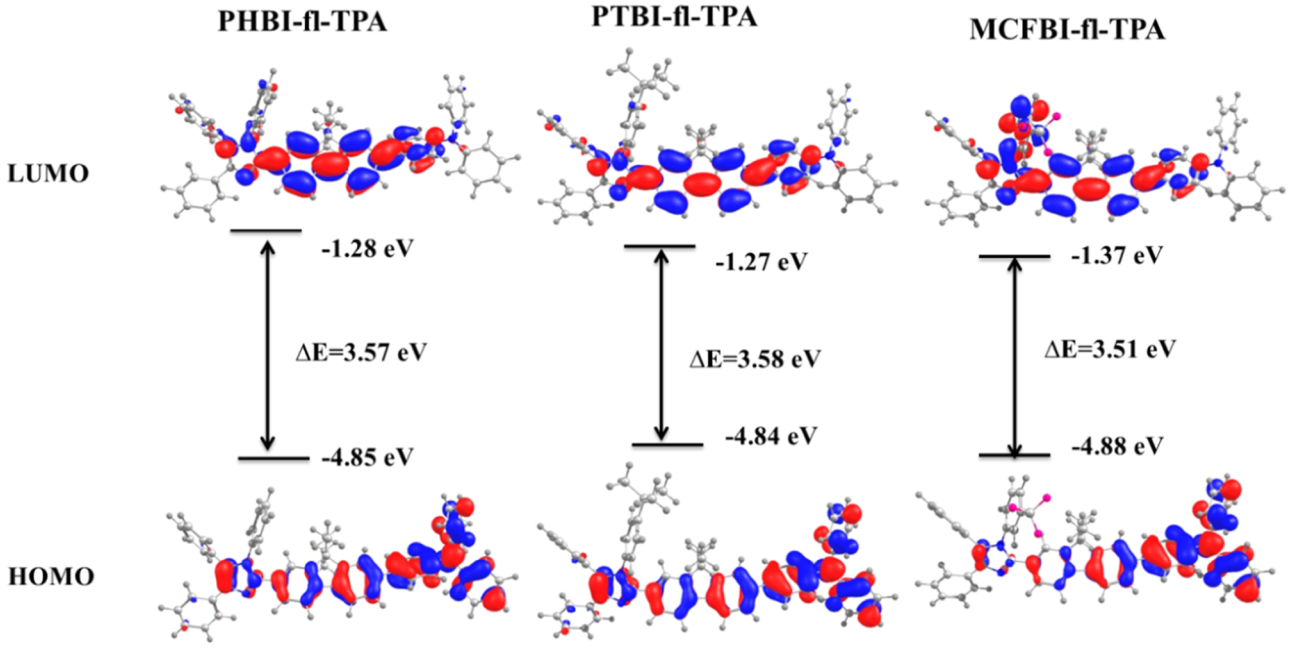

Figure 3. Density of electron of FMO of BI-fl-TPA derivatives.

process.[19−23] To encourage the RISC process, there must be minute energy difference between T_1 and S_1 (ΔE_{ST}) which is enough to boost the CT state which reveals the complete separation between highest occupied molecular orbital (HOMO) and lowest unoccupied molecular orbital (LUMO). However, TADF phenomena are sensitive to quench the triplet excitons, as a result drop in efficiency and limited lifetime of devices in the EL process.[24−27] So, the unique excited state is a HLCT process that conjoins the properties of local and CT states. The locally excited (LE) state assures the greater fluorescence quantum yield (η_{pl}), while the CT state assures a high exciton consumption rate. Theoretically HLCT materials can achieve 100% by using the excitons.[28] Furthermore, the LE state originates from the HLCT materials and therefore the emission spectrum is narrower and color purity of the devices is greater. Due to the presence of both states in HLCT materials, the overlap of HOMO and LUMO must be appearing, and the stiffness of molecules must be low. Better color gamut and diminished power depletion in displays and lighting is obtained with the help of deep-blue emitters based OLEDs. The high performance deep-blue emitters with satisfying the National Television (NTSC)/EBU standard values are still bottleneck for the smart displays and lightings. Tang et al., in 2015, built a donor−acceptor (D−A) molecule (PMSO), using a weak donor such as phenanthroimidazole and a moderate acceptor such as a sulfone, and obtained a maximum EQE of 6.85% for the doped device.[29] Ma et al. in 2019 constructed D−A kind molecules

https://doi.org/10.1021/acs.jpcc.3c00790
J. Phys. Chem. C 2023, 127, 10291−10302

Table 1. FMO and Energy Levels in the Excited States of BI-fl-TPA Derivatives

fluorophore	HOMO (eV)	LUMO (eV)	ΔE (eV)	S_1 (eV) (gas)	T_1 (eV) (gas)	oscillatory strength (f)
PHBI-fl-TPA	−4.8529	−1.2789	3.5740	3.1717	2.4755	1.3721
PTBI-fl-TPA	−4.8439	−1.2666	3.5773	3.1700	2.4694	1.3939
MCFBI-fl-TPA	−4.8784	−1.3660	3.5124	3.1328	2.4799	1.1150

termed DFPBI and TFPBI as emitters exhibited more EQEs of 4.18 and 5.74% with (0.154, 0.042) and (0.152, 0.054) CIE coordinates, respectively.[5] These consequences show that the HLCT is still the bottleneck for deep-blue emitters. Hence, the twisting nature and strength of D and A is a prime factor to modulate the HLCT states and ultimately improves the EQE of the device.

This work presents the blue fluorophores, twisted donor-π-acceptor (D-π-A) molecules, in which triphenylamine (TPA) act as a donor, 9,9-diethyl fluorene act as a π spacer, and benzilimidazole acts as an acceptor unit shown in Figure 1. The π spacer enhances the rigidity of the molecule which provides the necessary boldness to the molecule, which satisfies the contribution of the LE character and improves the efficiency of the molecules. The configurations of the doped device with ITO/PEDOT:PSS (50 nm)/PVK/1, 3, 5, 7.5, 10, 12.5, 15, 17.5, and 100 wt % PHBI-fl-TPA, PTBI-fl-TPA, and MCFBI-fl-TPA blended in TCTA/TPBi (20 nm)/LiF (1 nm)/Al (200 nm) results decrease in aggregation which is coming from emission quenching and distribute the balance charge carrier across the emission zone, and therefore, it increases the EL performance. The best performing 15 wt % MCFBI-fl-TPA-based device displays a maximum luminance of 3290 cd/m^2. The device illustrates 8.2 lm W^{-1} of power efficiency (PE), 7.9 cd A^{-1} of current efficiency (CE), and 3.5% of high EQE with (0.20, 0.23) coordinates of CIE of the device emits blue color. Furthermore, OLED devices comprise emitters PHBI-fl-TPA and PTBI-fl-TPA which exhibited EQEs of 1.3 and 2.0% with respective doping concentrations of 3 and 10 wt %. The CIE coordinates are (0.22, 0.18) and (0.18, 0.16) for the same doping concentration of the respective fluorophores.

THEORETICAL CALCULATIONS

To study the molecular electronic structures of the designed fluorophores, DFT calculations were carried out by using the basis set of the B3LYP/6-31G(d,p) method.[30,31] The optimized structures of BI-fl-TPA fluorophores with a dihedral angle are depicted in Figure 2. The dihedral angle shows that all the fluorophores having own twisted conformations, indicating non-coplanarity of the molecules. It is documented that the twisted confirmations of the fluorophores are emissive in the region of deep-blue to blue range.[32−34] The frontier molecular orbitals (FMO) with corresponding values are shown in Figure 3. The energy levels of HOMO, LUMO, energy band gaps between HOMO and LUMO (E_g), and excited states of energy level are calculated and summarized in Table 1. The HOMOs of the fluorophores show similar FMO distribution which are mostly located on the electron-donating TPA moiety and distributed over 9,9-diethyl fluorene aromatic rings and five-membered imidazole rings. However, the LUMOs are localized on the 9,9-diethyl fluorene bridge and imidazole moiety. In addition, the LUMO of MCFBI-fl-TPA also located on the N1-substituted meta connected tri-fluorine ($-CF_3$) phenyl ring because of the electron-withdrawing nature of the $-CF_3$ group. By varying the functionality at N1-bearing imidazole, the FMOs and theoretical energy band gaps of the fluorophores can be tuned and thus materials will show emission in the range of deep-blue to blue region. Furthermore, the transition from HOMO−LUMO + 1 also significantly contributed to the lowest transition for all the fluorophores validated by TD-DFT. The computed vertical transition, major contribution between HOMO−LUMO and oscillatory strength (f) are summarized in Table ST2. The theoretically absorption spectra were calculated by using TD-DFT with changing the exchange correlation functional. The simulated absorption spectra of these fluorophores in the gas phase and dichloromethane (DCM) phase are shown in Figure S22, which clearly reveals that the theoretical results of all the materials are in positive negotiation with preliminary studies. The CIE of the fluorophores were given in the Supporting Information (SI4 in the Supporting Information). Furthermore, to understand the RISC in deep-blue emissive materials, the excited state of the singlet and triplet states was analyzed by using TD-DFT calculations. The energy levels (S_1−S_{10} and T_1−T_{10}) of all the fluorophores are shown Figure S21. Very small differences in energies of 0.004 eV (T_4−S_1), 0.003 eV (T_4−S_1), and 0.058 eV (T_3−S_1) were noticed for PHBI-fl-TPA, PTBI-fl-TPA, and MCFBI-fl-TPA, respectively, and the energy difference between the T_1 and T_2 is large. The small difference between triplet and singlet energies and large difference between triplet (T_1−T_2) assume that the possibility of the RISC from triplet to singlet state.

For more discernment, we screened the molecules by breaking the carbon−carbon bond for free rotation (by replacing fluorene into diphenyl) of molecule. By analyzing the theoretical calculation, it is observed that if the molecule has free rotation, the wavelength of the molecule is shifted more toward the lower wavelength which is displayed in Figure S23 and their computed vertical transition, and the major contribution between HOMO−LUMO and oscillatory strength (f) is summarized in Table ST4.

To distinguish more about the transitions from ground (S_0) to excited (S_n) states of emissive materials to gratify the HLCT character, a multifunctional wavefunction analyzer (Multiwfn) was used. The natural transition orbitals (NTOs) of HONTOs and LUNTOs of the fluorophores were also calculated to know the electronic transitions of excited state as well as the hybrid splitting character from interstate coupling of LE and CT state to form the HLCT character (Tables ST7, ST9, and ST11). The design of HLCT is promoted by the index of Δr (average of hole to electron distance: r < 2.0 Å represents LE and r > 2.0 Å represents CT) and designates the behavior of LE and CT (Tables ST6, ST8, and ST10). The LE and CT excitation associated with short and large distance, respectively. The increasing % LE character and hybridization of LE with CT component reveals high photoluminescence quantum yield (PLQY) which leads to an increase in the device performance.

SYNTHESIS

The synthesis of blue emissive materials PHBI-fl-TPA, PTBI-fl-TPA, and MCFBI-fl-TPA, employs TPA as the donor (D) and

https://doi.org/10.1021/acs.jpcc.3c00790
J. Phys. Chem. C 2023, 127, 10291−10302

Scheme 1. Synthetic Routes of the BI-fl-TPA Derivatives

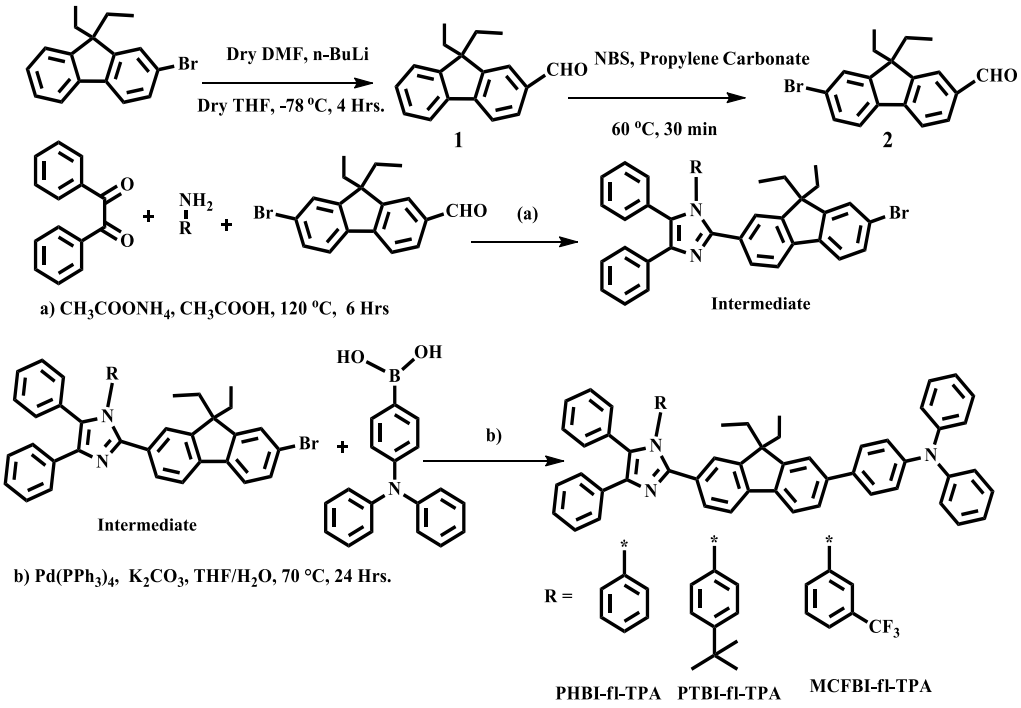

benzilimidazole as the acceptor (A), benzilimidazole (BI) having different substituent at N1-position and their synthetic route is shown in Scheme 1. The intermediates and the synthesized products are confirmed by the spectroscopy method such as NMR (^{1}H, ^{13}C), high resolution mass spectroscopy (HRMS), and single-crystal XRD.

RESULTS AND DISCUSSION

Thermogravimetric Analysis. The thermal stability of the blue emissive materials were studied by thermogravimetric analysis (TGA). The test was carried out from ambient temperature to 600 °C with a heating rate of 10 °C/min in an inert (N_2) atmosphere. The TGA curves of these fluorophores exhibited high decomposition temperature (T_d) of 5% weight

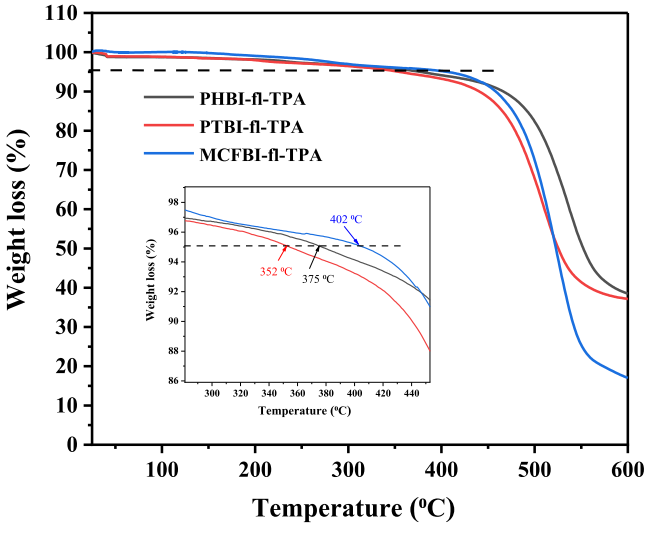

Figure 4. Thermogravimetric curves of PHBI-fl-TPA, PTBI-fl-TPA, and MCFBI-fl-TPA.

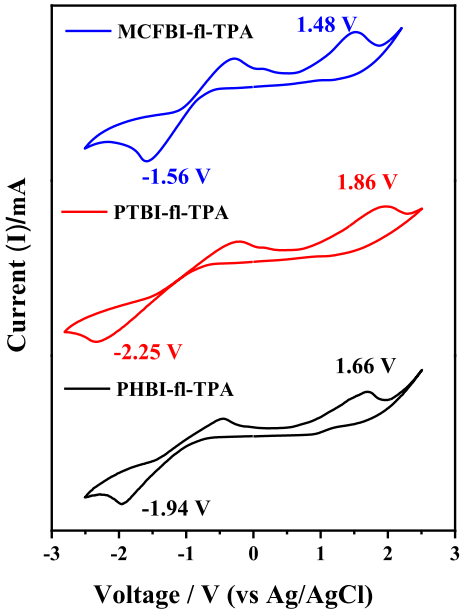

Figure 5. Cyclic voltammograms of PHBI-fl-TPA, PTBI-fl-TPA, and MCFBI-fl-TPA at room temperature.

Table 2. Key Data of the Electrochemical Analysis of BI-fl-TPA Derivatives

fluorophore	E_{ox} [a] (V)	E_{red} [b] (V)	HOMO (eV)	LUMO (eV)	E_g [c] (eV)
PHBI-fl-TPA	1.66	−1.94	−6.06	−2.46	3.68
PTBI-fl-TPA	1.86	−2.25	−5.88	−2.15	3.73
MCFBI-fl-TPA	1.48	−1.56	−6.26	−2.84	3.42

[a]The onset oxidation potential. [b]The onset reduction potential. [c]Electrochemical band gap determined from CV (E_g = HOMO−LUMO).

https://doi.org/10.1021/acs.jpcc.3c00790
J. Phys. Chem. C 2023, 127, 10291−10302

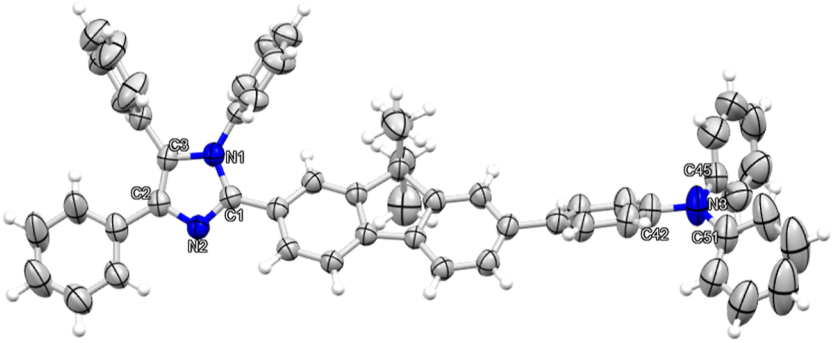

Figure 6. ORTEP diagram of ball and stick models of the PHBI-fl-TPA crystal (50% probability ellipsoids). N atoms blue in color (CCDC 2196184).

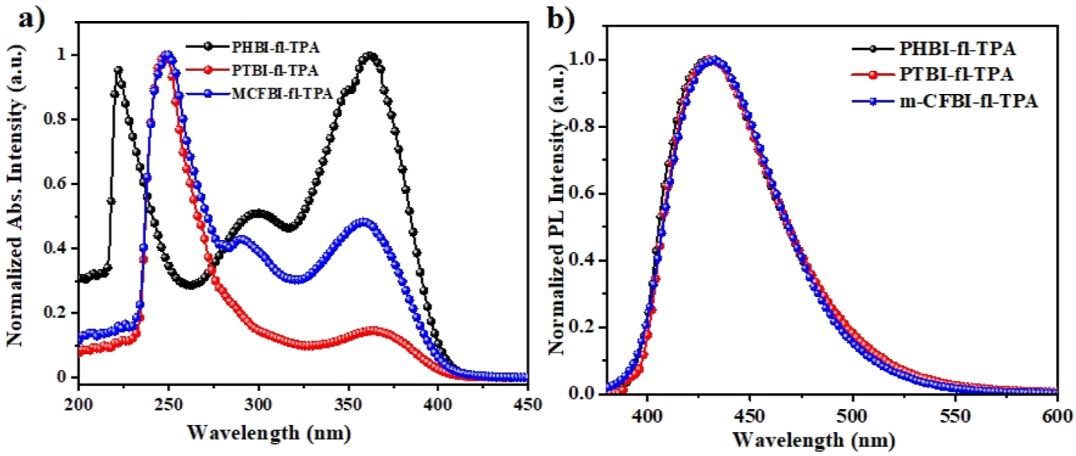

Figure 7. (a) Normalized UV−vis absorption spectra and (b) PL spectra in THF solution (10^{-5} M).

Table 3. Key Photophysical Properties of BI-fl-TPA Fluorophores

		solution			solid			
compounds	[a]T_d °C	λ_{abs} (nm)	λ_{PL} (nm)	CIE (x, y)	λ_{ex} (nm)	λ_{PL} (nm)	CIE (x, y)	PLQY solution/thin film %
PHBI-fl-TPA	375	222, 298, 361	430	(0.15, 0.05)	403	443	(0.15, 0.10)	88/45
PTBI-fl-TPA	352	248, 363	431	(0.15, 0.05)	412	445	(0.15, 0.09)	54/15
m-CFBI-fl-TPA	402	250, 289, 360	436	(0.15, 0.06)	408	440	(0.15, 0.13)	43/30

[a]Thermal decomposition temperature corresponding to 5% weight loss.

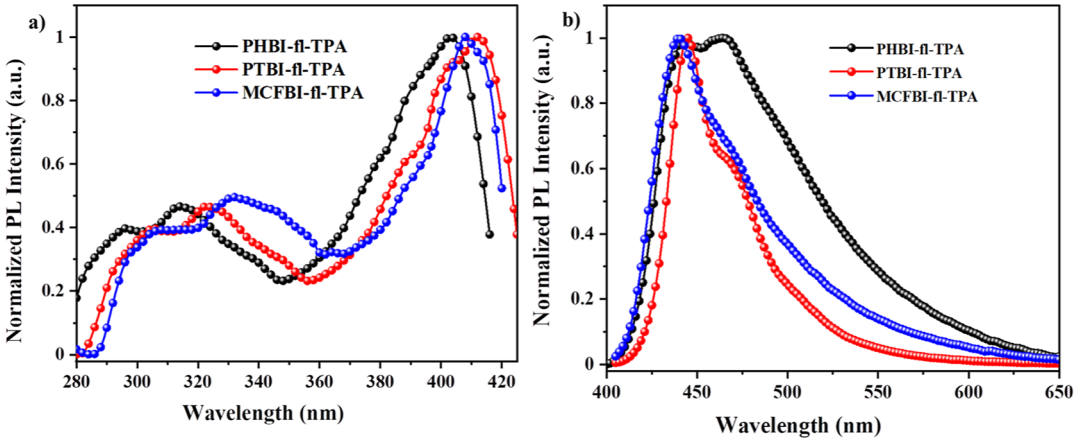

Figure 8. (a) Normalized PL excitation (b) emission of the BI-fl-TPA fluorophores in the solid state.

loss ranging from 352 to 402 °C displayed in Figure 4. The 5% weight loss for PHBI-fl-TPA, PTBI-fl-TPA, and MCFBI-fl-TPA were found to be 375, 352, and 402 °C, respectively, which are comparable to 10% weight loss of 340 °C of PPI and 430 °C of TPBi.[35,36] Among all, MCFBI-fl-TPA material displayed highest T_d of 402 °C and this could be ascribed due

https://doi.org/10.1021/acs.jpcc.3c00790
J. Phys. Chem. C 2023, 127, 10291−10302

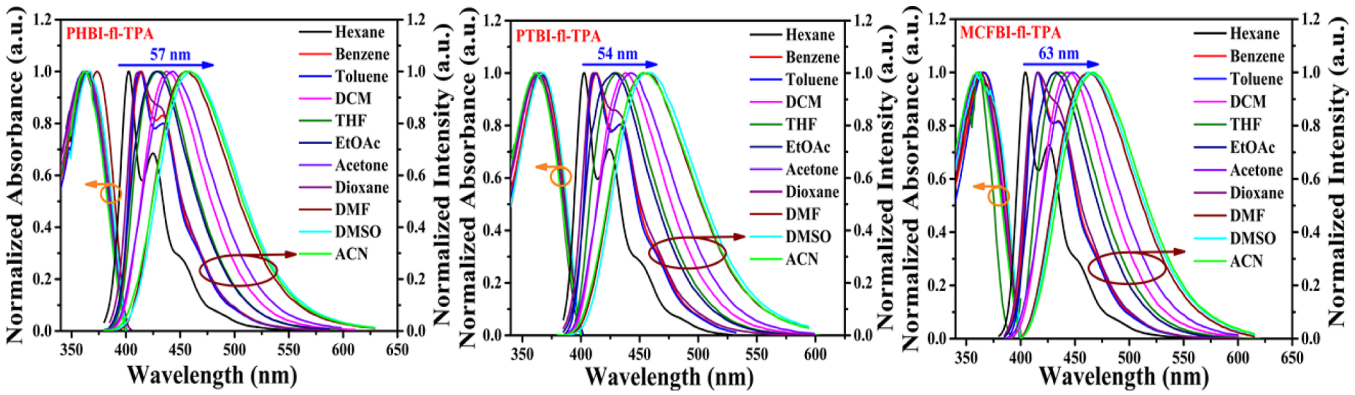

Figure 9. Normalized UV−vis absorbance and PL spectra of BI-fl-TPA derivatives in various solvents.

Table 4. Key Photophysical Properties of PHBI-fl-TPA, PTBI-fl-TPA, and MCFBI-fl-TPA

		PHBI-fl-TPA			PTBI-fl-TPA			MCFBI-fl-TPA		
solvents	Δf	λ_{abs} (nm)	λ_{em} (nm)	Stokes' shift (cm^{-1})	λ_{abs} (nm)	λ_{em} (nm)	Stokes' shift (cm^{-1})	λ_{abs} (nm)	λ_{em} (nm)	Stokes' shift (cm^{-1})
hexane	0.0012	361	401	2763	365	402	2521	364	404	2720
benzene	0.002	361	413	3487	363	412	3276	364	415	3376
toluene	0.0131	361	414	3546	365	411	3066	364	415	3376
DCM	0.220	361	437	4741	365	438	4566	362	444	5101
THF	0.210	361	430	4445	363	430	4292	362	436	4688
EtOAc	0.200	362	428	4259	364	428	4108	361	431	4498
acetone	0.284	361	442	5076	364	442	4848	361	448	5379
dioxane	0.022	361	433	4606	363	411	3217	361	416	3662
DMF	0.276	372	454	4855	363	456	5618	360	462	6132
DMSO	0.264	365	457	5575	367	458	5413	360	463	6179
ACN	0.305	362	458	5790	362	456	5694	360	467	6364

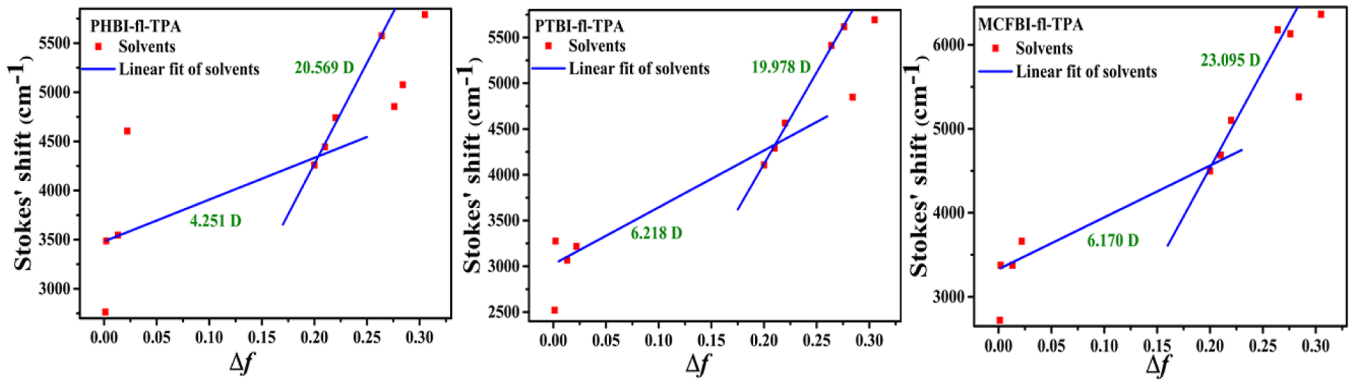

Figure 10. Lippert−Mataga model in various solvents from non-polar to polar for BI-fl-TPA derivatives.

to the company of superior thermal stability of the imidazole ring and aromatic backbone. The obtained thermal data reveal that currently investigated blue emissive materials possesses high thermal stability and it is the fundamental requirements for organic electronic since high T_d enhances the lifetime of the devices.

Electrochemical Properties. The redox properties of blue emissive materials were investigated by using cyclic voltammetry (CV) measurements in dimethylformamide (DMF) solution at a scanning rate of 100 mV/s and supporting electrolyte as tetrabutylammonium perchlorate (Bu_4NClO_4) 0.1 M. Figure 5 shows CV curves of all the blue emissive materials and found that these fluorophores possesses a distinct oxidation and reduction potentials, which implies that materials may have bipolar carrier transporting properties. The first oxidative potentials and reductive potentials are found to be in the vicinity of 1.48 to 1.86 and −1.56 to −2.25 V, respectively. By considering onset potentials, the energy levels of HOMO and LUMO were examined by using de Leeuw et al. eqs 1 and 2.[37]

$$E_{HOMO} = -(E_{ox}^{onset} + 4.4)\ eV \quad (1)$$

$$E_{LUMO} = -(E_{red}^{onset} + 4.4)\ eV \quad (2)$$

The HOMO/LUMO energy levels for PHBI-fl-TPA, PTBI-fl-TPA, and MCFBI-fl-TPA were calculated and found to be −6.06/−2.46, −5.88/−2.15, and −5.26/−2.84 eV with difference between energy of HOMO and LUMO (E_g = HOMO−LUMO) of 3.68, 3.73, and 3.42 eV, respectively, and their calculated data are summarized in Table 2. The proper

https://doi.org/10.1021/acs.jpcc.3c00790
J. Phys. Chem. C 2023, 127, 10291−10302

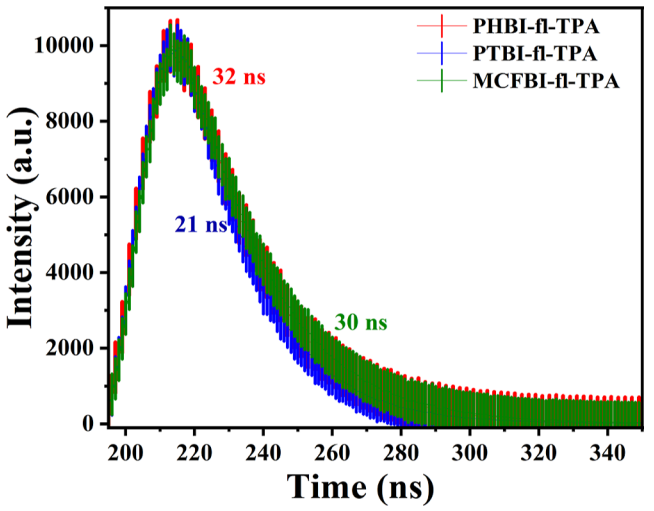

Figure 11. Transient PL decay curves of three emitters in $CHCl_3$ solution (concentration 10^{-6} M).

agreement between HOMO−LUMO energy levels is advantageous for injection and transportation of charge carriers (hole and electrons) which moderates the accumulation of charge carriers at the boundaries among the emissive and nearby charge transporting layers of the device.[38] From Table 2, it was clear that the calculated band gaps examined by both theoretical and electrochemical analysis are in good alignment.

Single X-ray Structural Characterization. The ORTEP diagram of solid PHBI-fl-TPA (crystallize in monoclinic structure) characterized by the single-crystal X-ray diffraction technique is shown in Figure 6. The planes of the imidazole ring and N1 connected phenyl groups were twisted appreciably proportionality to each other with angle C1−N1−C16 (128.2°) and C3−N1−C16 (124.2°). It reveals that the bulkier group of fluorene side more hindered side as compared to the other side of the benzil group. Therefore, the benzilimidazole ring was remarkably twisted as compared to the fluorene carbon and TPA carbon. The distance between the bond of the N1 atom and phenyl carbons are almost in the range of 1.44 Å. The bond angles of the TPA are almost in the

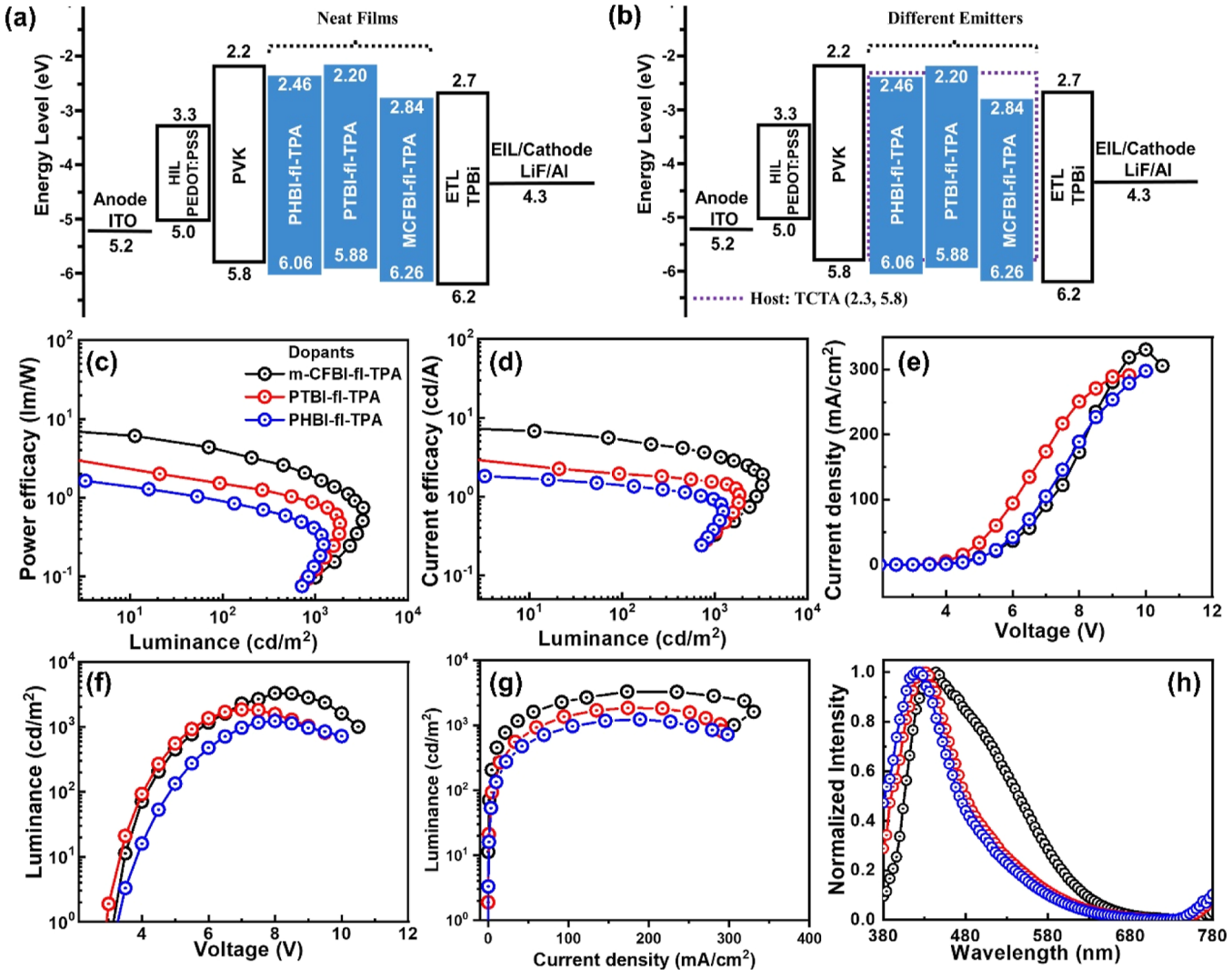

Figure 12. Energy-level diagrams of (a) neat-films-based device and (b) TCTA-based devices doped with different emitters PHBI-fl-TPA, PTBI-fl-TPA, and MCFBI-fl-TPA. EL properties of studied devices from the perspective of (c) power efficacy vs luminance, (d) current efficacy vs luminance, (e) current density vs voltage, (f) luminance vs voltage, (g) luminance vs current density, and (h) EL spectra of neat-films-based devices and TCTA-doped devices.

https://doi.org/10.1021/acs.jpcc.3c00790
J. Phys. Chem. C 2023, 127, 10291−10302

Table 5. Summarized EL Properties of Studied Devices with Different Concentrations of Emitters

			@100, 1000 cd/m^2 and maximum values				
dopants	dopant con. (wt %)	V_{on} (V)	power efficacy (lm/W)	current efficacy (cd/A)	EQE (%)	CIE$_{xy}$@100 cd/m^2	L_{max} cd/m^2
m-CFBI-fl-TPA	1	3.0	1.4/0.9/2.5	1.7/1.6/2.4	0.8/1.2/2.4	(0.18, 0.15)	1730
	3	2.9	1.5/1.0/2.6	1.9/1.7/2.5	1.9/1.2/1.9	(0.19, 0.16)	1926
	5	2.8	2.1/1.3/4.0	2.6/2.3/3.8	2.3/1.6/2.5	(0.19, 0.16)	2882
	7.5	2.7	2.2/1.2/5.3	3.2/2.4/5.1	2.4/2.0/2.4	(0.19, 0.18)	3526
	10	2.9	2.6/1.4/5.6	3.7/2.7/4.9	2.8/2.2/3.0	(0.19, 0.18)	3246
	12.5	3.0	3.6/1.6/7.3	4.8/3.0/7.0	2.8/2.4/3.1	(0.20, 0.23)	2921
	15	3.0	4.1/1.8/8.2	5.4/3.4/7.9	3.1/2.7/3.5	(0.20, 0.23)	3290
	17.5	3.1	2.1/0.7/3.9	3.0/1.5/4.3	1.7/1.3/2.0	(0.19, 0.21)	1755
	100	3.0	1.3/-/1.3	1.7/-/1.9	0.6/-/0.7	(0.28, 0.48)	927
PTBI-fl-TPA	1	2.7	0.8/-/1.3	1.0/-/1.3	1.1/-/1.1	(0.17, 0.14)	995
	3	2.7	1.1/0.7/1.9	1.5/1.4/1.8	1.6/1.2/1.6	(0.18, 0.14)	1560
	5	2.8	1.3/0.8/2.5	1.7/1.5/2.3	1.7/1.3/1.8	(0.18, 0.15)	1665
	7.5	2.8	1.3/0.8/2.6	1.8/1.6/2.4	1.7/1.3/1.9	(0.18, 0.15)	1728
	10	2.9	1.5/0.9/3.2	1.9/1.5/3.1	1.8/1.3/2.0	(0.18, 0.16)	1845
	12.5	3.0	0.9/0.4/2.1	1.3/0.9/2.0	1.2/0.8/1.2	(0.19, 0.16)	1180
	100	3.0	1.0/-/1.1	1.3/-/1.5	0.5/-/0.6	(0.23, 0.42)	713
PHBI-fl-TPA	1	3.0	0.8/0.4/1.4	1.3/0.8/1.6	1.1/0.6/1.1	(0.19, 0.14)	1090
	3	3.1	0.9/0.4/1.6	1.4/0.9/1.8	1.3/0.9/1.3	(0.22, 0.18)	1230
	5	3.3	0.7/0.3/1.1	1.3/0.8/1.4	1.1/0.7/1.1	(0.21, 0.17)	1240
	7.5	3.5	0.8/0.3/1.0	1.0/0.8/1.1	1.0/0.6/1.0	(0.21, 0.17)	1270
	10	3.6	0.6/0.3/0.8	1.0/0.7/1.0	0.9/0.6/1.0	(0.21, 0.17)	1160
	100	3.6	0.2/-/0.2	0.4/-/0.4	0.2/-/0.2	(0.21, 0.38)	702

range of 120° and distance of the bond between N3 atom and C45 is 1.43 Å, between N3 atom and C42 is 1.40 Å, and between N3 atom and C51 is 1.45 Å. The key data of the crystal and corresponding bond length and angles from single-crystal XRD data are displayed in Figure 6 and Table ST12.

Photophysical Properties. The deep blue BI-fl-TPA fluorophores are synthesized and their absorption and emission spectra are examined by employing the UV−vis spectrophotometer and spectrofluorometer. The absorption and emission spectra were documented in tetrahydrofuran (THF) solution (10^{-5} M) as shown in Figure 7, and the summarized data are tabulated in Table 3. The similar absorption band of fluorophores exhibits around in the region of 222−363 nm in the solution phase (Figure 7a). It reveals that the absorption spectra nearby 222−298 nm which may be ascribed due to the $\pi-\pi^*$ transitions of benzilimidazole and phenyl rings.[39,40] However, well-built absorption spectra at around 360−363 nm may be ascribed due to the transitions of $\pi-\pi^*$ as well as intramolecular charge transfer (ICT) among benzilimidazole and TPA.[41] The emission spectra of the fluorophores in solution (Figure 7b) demonstrate the peaking wavelength around 430, 431, and 436 nm for PHBI-fl-TPA, PTBI-fl-TPA, and MCFBI-fl-TPA, respectively. Also, the solid emission spectra are showing unusual behavior from those in solution because of the formation of excimer or exciplex in the solid states.[42−46] The fluorophores showed deep blue emissions under UV in the THF solution and also their CIE color gamuts favor the NTSC standard and are displayed in Figure S20. The corresponding CIE color coordinates (x and y) of the fluorophores are presented in Table 3. However, the PTBI-fl-TPA and MCFBI-fl-TPA shows inappreciable red-shift emission in solid states (Figure 8b) compared to the solution. This statement reveals that the communication among the molecules in the solid phase were restrained efficaciously because of a definite framework and highly twisted geometries of the synthesized fluorophores.[47]

By using the integrating sphere, the absolute quantum yields (Φ) of the BI-fl-TPA fluorophores were examined both in solution and neat thin film which are summarized in Table 3. All the fluorophores showed good quantum yield and which is a requisite for proficient blue OLEDs. The quantum yield of PHBI-fl-TPA, PTBI-fl-TPA, and MCFBI-fl-TPA in solution and thin film are conveyed 88/45, 54/15, and 43/30%, respectively. The doping concentration of 15% of MCFBI-fl-TPA in the film displays 64.4% of PLQY. The fluorophores are showing higher quantum yield which reveals the survival of dual emission of LE and CT character.

Solvatochromism. To further study the characteristics of fluorophores with changing solvent polarity, the thoroughly studied done by solvatochromism experiments. The fluorophores test by different solvents (non-polar to polar) was selected to further study the ICT. The absorbance spectra and PL emission of new born fluorophores were performed in different solvents: hexane, benzene, toluene, DCM, THF, ethylacetate (EtOAc), acetone, dioxane, DMF, dimethyl sulfoxide (DMSO), and acetonitrile (ACN), as shown in Figure 9.

From Figure 9, it was found that by changing the polarity of the solvent from non-polar to polar, the fluorophores show very negligible influence on the absorbance spectra due to very small change in the dipole moment at the ground state.[48] Whereas, PL emissions clearly indicate redshifts of 57, 53, and 64 from non-polar to polar for PHBI-fl-TPA, PTBI-fl-TPA, and MCFBI-fl-TPA, respectively, with broadening in the PL spectra increase full width half maxima from hexane (less polar) to ACN (high polarity) solvents indicates that a remarkable change in dipole moment results in CT in excited states of all fluorophores.[49] The detailed photophysical data are tabulated in Table 4. Furthermore, it was found that the PL emission spectra in non-polar solvents (hexane, benzene, and toluene) show two fine vibrational structure spectra which show the LE feature of excited states in a non-polar solvent. With

https://doi.org/10.1021/acs.jpcc.3c00790
J. Phys. Chem. C 2023, 127, 10291−10302

progressively polarity after toluene, the peak turns into non-vibrational and keeps this until using ACN which results CT in excited states.[50] This event may indicate that the simultaneous presence of both close lying LE and CT state, slight change in the solvent polarity CT character dominate in excited states.[51] In addition, to study the enhancement of solvent on to the photophysical properties of fluorophores can also be accepted by using the Lippert−Mataga equation, which thoroughly deliberated the communication between the solvent and the dipole moment of the solute in the ground state (S_0) and the lowest excited states (S_1). The Lippert−Mataga set out the Stokes' shift (cm^{-1}) as function of change in dipole moment ($\Delta\mu_{ge} = \mu_e - \mu_g$) represented by eqs 3 and 4.[52,53]

$$hc(\nu_a - \nu_f) = hc\,(\nu_a^o - \nu_f^o) - \frac{2\,(\mu_e - \mu_g)^2}{a^3} f(\varepsilon, n) \quad (3)$$

where $(\nu_a^o - \nu_f^o)$ stands for Stokes' shifts (in cm^{-1}) between the absorption and emission maxima [$\nu_a^o = 1/\lambda_{abs}$ (max), $\nu_f^o = 1/\lambda_{em}$ (max)], h and c stand for Planck's constant and velocity of light, respectively, and μ_e and μ_g stands for dipole moment in excited states and ground states.

$$\Delta f = f(\varepsilon, n) = \frac{\varepsilon - 1}{2\varepsilon + 1} - \frac{n^2 - 1}{2n^2 + 1} \quad (4)$$

$$a = \left(\frac{3M}{4N\pi d}\right)^{1/3}$$

where Δf and α stand for the solvents orientation polarizability and solvent cavity radius, derived from Avogadro's number (N), the molecular weight (M), and the density (d = 1.0 g/cm^3); ε and n stand for[54] solvent dielectric and solvent refractive indices, respectively. The plot was drawn using Stokes' shift as a function of orientation polarizability (Δf).[54,55] Figure 10 represents the non-linear relationship of Stokes' shift and orientation polarizability of PHBI-fl-TPA, PTBI-fl-TPA, and MCFBI-fl-TPA in different solvents, and corresponding data are summarized in Table 4. From Figure 10, the two-segmental lines of the fluorophores in the low polarity solvents show small dipole moments (μ_g) of 4.25, 6.21, and 6.17 D and large dipole moments of 20.56, 19.97, and 23.09 D noted for PHBI-fl-TPA, PTBI-fl-TPA, and MCFBI-fl-TPA, respectively, can be associated with the emissive HLCT state. The small and large dipole moments of the fluorophores attributed to LE and CT components, respectively, and the co-emission of both states supports the HLCT character of the fluorophores.

Transient PL decay curve of three emitters in $CHCl_3$ solution (concentration 10^{-6} M) was carried out utilizing the time correlated single photon counting method under the excitation of around 365 nm in order to further explore the parameters of the excited state. As shown in Figure 11, the PHBI-fl-TPA, PTBI-fl-TPA, and MCFBI-fl-TPA emitters revealed a single exponential decay curve with prompt lifespans of 32, 21, and 30 ns, respectively, which suggested that the emission is coming from the single excited state. Hence, the HLCT property of the S1 state is suggested by the one lifetime decay profile, which shows that the LE and CT states are highly mixed or hybridized in the S1 state.[29,56]

Electroluminescent Properties. OLEDs were fabricated by using synthesized blue emitters PHBI-fl-TPA, PTBI-fl-TPA, and MCFBI-fl-TPA in emission layers (EMLs) to scrutinize the alliance between the device performance and molecular properties. The device configuration using emitters with an ITO/PEDOT:PSS (50 nm)/PVK/PHBI-fl-TPA, PTBI-fl-TPA, and MCFBI-fl-TPA/TPBi (20 nm)/LiF (1 nm)/Al (200 nm) device architecture. ITO-coated glass and LiF/Al act as an anode and cathode, respectively, whereas TPBi is an electron transporting layer shown in Figure 12. When potential is enforced, holes and electrons are injected from the respective anode and cathode electrode. In the active emissive layer of OLED device, the recompensation of holes and electron results to emits blue photon emission. The results obtained from OLED device execution which confines the turn on voltage, CE, PE, CIE co-ordinates, electroluminescent peak, and maximum luminance are depicted in table. The EL spectra of the device are very similar to PL spectra in the solution phase deposition which depicted in Figure 12. The current density−voltage and luminance−voltage of the EL device of all the emitters are shown in Figure 12. The different doping concentration of the respective emitters, PHBI-fl-TPA, and PTBI-fl-TPA are shown in Figures S24 and S25. The MCFBI-fl-TPA OLED device shows low turn-on voltage (V_{on}) of 3.0 V for EL and exhibits a CE of 7.9 cd/A with a maximum luminance of 3290 cd/m^2 are shown in Figures S26. The chromaticity coordinates (x, y) of the device are found to be (0.20, 0.23) which corresponds to the sky-blue color and reaches a maximum EQE of 3.5%.

The device efficiency is achieved in this work because of its high values of PLQY for solution simultaneously with the successful choose the hole transporting layer, hole blocking layer, and electron transporting layer which reflected in Figure 12. The recombination area provides the suitable charge carrier balance of these materials and is especially important in the context of the relatively high hole mobility in the emissive layer. As the non-doped devices exposed destitute EL properties due to the formation of aggregates, carrier quenching as well as non-radiative recombination. We further simulated the doped device with the configurations of ITO/PEDOT:PSS (50 nm)/PVK/1, 3, 5, 7.5, 10, 12.5, 15, 17.5, and 100 wt % PHBI-fl-TPA, PTBI-fl-TPA, and MCFBI-fl-TPA doped in TCTA/TPBi (20 nm)/LiF (1 nm)/Al (200 nm) results decreasing in aggregation caused emission quenching and balance charge carrier distribution across the emission zone, and therefore, it increases the EL performance. In addition, the emission peak observed at 480−580 nm in the OLED device produced by MCFBI-fl-TPA could be attributed to the formation of excimer production in solid-state thin films. However, it is important to note that the shape and position of the EL spectra in OLEDs can be influenced by various factors such as device fabrication conditions, temperature, and voltage applied to the device.

Among all, the best performing 15 wt % MCFBI-fl-TPA-based OLED device shows a maximum luminance of 3290 cd/m^2, PE of 8.2 lm/W, CE of 7.9 cd/A, and high EQE of 3.5% with chromaticity coordinates (x, y) of the device are found to be (0.20, 0.23) emits sky-blue color. Furthermore, an OLED device comprises emitters PHBI-fl-TPA and PTBI-fl-TPA exhibited EQE of 1.3 and 2.0% with respective doping concentration of 3 and 10 wt %. The CIE coordinates of (0.22, 0.18) and (0.18, 0.16) for the same doping concentration of the respective fluorophores emits blue emission. The summarized EL properties of studied devices with different concentrations of PHBI-fl-TPA, PTBI-fl-TPA, and MCFBI-fl-TPA shown in Table 5.

The current density−voltage and luminance−voltage of the EL device plots of solution processed deep blue emission

https://doi.org/10.1021/acs.jpcc.3c00790
J. Phys. Chem. C 2023, 127, 10291−10302

OLED device with different doping concentrations in the TCTA host. The CIE chromaticity and maxima EL spectra peaking around 400−450 nm, which are well matched with those of standard blue emission satisfied by the NTSC standard. Additionally, it is notable that EL spectra of the device are well resembled with PL spectra, which are recorded in DCM solution. It results the orderly dispersion of the dopant molecules into appropriate host materials with the annihilation of aggregation in thin films and predominant source of emission from the emitter molecules.

CONCLUSIONS

We have synthesized three thermally stable fluorene π-spacer fluorophores by attaching with benzilimidazole and TPA with HLCT behavior. The synthesized blue-emitting fluorophores reveal good PLQY in both solution and thin-film matrix which leads to enhanced device performance. The computational study (DFT and NTOs) and experiments (solvatochromism and plot of Lipper−Mataga) represent these materials as hybrid LE and CT states. Furthermore, these fluorophores were worn as dopant materials, and they were fabricated as doped and undoped device. Among all, the best performing 15 wt % MCFBI-fl-TPA-based OLED device illustrates a maximum luminance of 3290 cd/m^2. The device shows 8.2 lm W^{-1} of PE, 7.9 cd A^{-1} of CE, and 3.5% of high EQE with (0.20, 0.23) of CIE coordinates of the device emitting a blue color.

ASSOCIATED CONTENT

Supporting Information

The Supporting Information is available free of charge at https://pubs.acs.org/doi/10.1021/acs.jpcc.3c00790.

Crystallographic data (CIF)

checkCIF report (PDF)

General information and measurements, computational details, device fabrication and measurements, synthesis of intermediates, NMR spectra (^{1}H and ^{13}C), HRMS spectra, CIE coordinates for the compounds in solutions and solid phase and their x and y coordinates in tabular form, theoretically calculated UV−vis absorption spectra and vertical transition compositions, NTOs calculation, atomic coordinates of all the fluorophores, device characterization, and PLQY and bond distance and bond length of the crystal (PDF)

AUTHOR INFORMATION

Corresponding Author

Sivakumar Vaidyanathan − *Department of Chemistry, Indian Institute of Technology Hyderabad, Kandi, Telangana 502285, India;* orcid.org/0000-0002-2104-2627; Email: vsiva@chy.iith.ac.in

Authors

Sandhya Rani Nayak − *Department of Chemistry, National Institute of Technology Rourkela, Rourkela 769 008 Odisha, India; Department of Chemistry, Indian Institute of Technology Hyderabad, Kandi, Telangana 502285, India*

Jaipal Devesing Girase − *Department of Chemistry, National Institute of Technology Rourkela, Rourkela 769 008 Odisha, India*

Mangey Ram Nagar − *Department of Materials Science and Engineering, National Tsing Hua University, Hsinchu 30013, Taiwan*

Jwo-Huei Jou − *Department of Materials Science and Engineering, National Tsing Hua University, Hsinchu 30013, Taiwan;* orcid.org/0000-0002-9413-0206

Complete contact information is available at: https://pubs.acs.org/10.1021/acs.jpcc.3c00790

Notes

The authors declare no competing financial interest.

ACKNOWLEDGMENTS

VS acknowledges SERB, Department of Science and Technology (DST), India (EMR/2016/002462).

REFERENCES

(1) Tang, C. W.; VanSlyke, S. A. Organic Electroluminescent Diodes. *Appl. Phys. Lett.* **1987**, *51*, 913−915.

(2) Ma, Y.; Zhang, H.; Shen, J.; Che, C. Electroluminescence from Triplet Metal—Ligand Charge-Transfer Excited State of Transition Metal Complexes. *Synth. Met.* **1998**, *94*, 245−248.

(3) Jou, J.-H.; Shen, S.-M.; Lin, C.-R.; Wang, Y.-S.; Chou, Y.-C.; Chen, S.-Z.; Jou, Y.-C. Efficient Very-High Color Rendering Index Organic Light-Emitting Diode. *Org. Electron.* **2011**, *12*, 865−868.

(4) Kim, S.; Kwon, H.-J.; Lee, S.; Shim, H.; Chun, Y.; Choi, W.; Kwack, J.; Han, D.; Song, M.; Kim, S.; et al. Low-Power Flexible Organic Light-Emitting Diode Display Device. *Adv. Mater.* **2011**, *23*, 3511−3516.

(5) Qiu, X.; Ying, S.; Wang, C.; Hanif, M.; Xu, Y.; Li, Y.; Zhao, R.; Hu, D.; Ma, D.; Ma, Y. Novel 9,9-Dimethylfluorene-Bridged D−π−A-Type Fluorophores with a Hybridized Local and Charge-Transfer Excited State for Deep-Blue Electroluminescence with CIEy ∼ 0.05. *J. Mater. Chem. C* **2019**, *7*, 592−600.

(6) Fan, Y.; Zhang, H.; Chen, J.; Ma, D. Three-Peak Top-Emitting White Organic Emitting Diodes with Wide Color Gamut for Display Application. *Org. Electron.* **2013**, *14*, 1898−1902.

(7) Sun, Y.; Giebink, N. C.; Kanno, H.; Ma, B.; Thompson, M. E.; Forrest, S. R. Management of Singlet and Triplet Excitons for Efficient White Organic Light-Emitting Devices. *Nature* **2006**, *440*, 908−912.

(8) Zheng, C.-J.; Wang, J.; Ye, J.; Lo, M.-F.; Liu, X.-K.; Fung, M.-K.; Zhang, X.-H.; Lee, C.-S. Novel Efficient Blue Fluorophors with Small Singlet-Triplet Splitting: Hosts for Highly Efficient Fluorescence and Phosphorescence Hybrid WOLEDs with Simplified Structure. *Adv. Mater.* **2013**, *25*, 2205−2211.

(9) Lee, S. J.; Park, J. S.; Yoon, K.-J.; Kim, Y.-I.; Jin, S.-H.; Kang, S. K.; Gal, Y.-S.; Kang, S.; Lee, J. Y.; Kang, J.-W.; et al. High-Efficiency Deep-Blue Light-Emitting Diodes Based on Phenylquinoline/Carbazole-Based Compounds. *Adv. Funct. Mater.* **2008**, *18*, 3922−3930.

(10) Schwartz, G.; Reineke, S.; Rosenow, T. C.; Walzer, K.; Leo, K. Triplet Harvesting in Hybrid White Organic Light-Emitting Diodes. *Adv. Funct. Mater.* **2009**, *19*, 1319−1333.

(11) Im, Y.; Byun, S. Y.; Kim, J. H.; Lee, D. R.; Oh, C. S.; Yook, K. S.; Lee, J. Y. Recent Progress in High-Efficiency Blue-Light-Emitting Materials for Organic Light-Emitting Diodes. *Adv. Funct. Mater.* **2017**, *27*, 1603007.

(12) Jou, J.-H.; Kumar, S.; Agrawal, A.; Li, T.-H.; Sahoo, S. Approaches for Fabricating High Efficiency Organic Light Emitting Diodes. *J. Mater. Chem. C* **2015**, *3*, 2974−3002.

(13) Wang, K.; Zhao, F.; Wang, C.; Chen, S.; Chen, D.; Zhang, H.; Liu, Y.; Ma, D.; Wang, Y. High-Performance Red, Green, and Blue Electroluminescent Devices Based on Blue Emitters with Small Singlet−Triplet Splitting and Ambipolar Transport Property. *Adv. Funct. Mater.* **2013**, *23*, 2672−2680.

(14) Chen, W.-C.; Lee, C.-S.; Tong, Q.-X. Blue-Emitting Organic Electrofluorescence Materials: Progress and Prospective. *J. Mater. Chem. C* **2015**, *3*, 10957−10963.
(15) Tagare, J.; Vaidyanathan, S. Recent Development of Phenanthroimidazole-Based Fluorophores for Blue Organic Light-Emitting Diodes (OLEDs): An Overview. *J. Mater. Chem. C* **2018**, *6*, 10138−10173.
(16) Uoyama, H.; Goushi, K.; Shizu, K.; Nomura, H.; Adachi, C. Highly Efficient Organic Light-Emitting Diodes from Delayed Fluorescence. *Nature* **2012**, *492*, 234−238.
(17) Kondakov, D. Y.; Pawlik, T. D.; Hatwar, T. K.; Spindler, J. P. Triplet Annihilation Exceeding Spin Statistical Limit in Highly Efficient Fluorescent Organic Light-Emitting Diodes. *J. Appl. Phys.* **2009**, *106*, 124510.
(18) Kondakov, D. Y. Triplet−Triplet Annihilation in Highly Efficient Fluorescent Organic Light-Emitting Diodes: Current State and Future Outlook. *Philos. Trans. R. Soc., A* **2015**, *373*, 20140321.
(19) Lee, J.-H.; Chen, C.-H.; Lee, P.-H.; Lin, H.-Y.; Leung, M.; Chiu, T.-L.; Lin, C.-F. Blue Organic Light-Emitting Diodes: Current Status, Challenges, and Future Outlook. *J. Mater. Chem. C* **2019**, *7*, 5874−5888.
(20) Chen, B.; Liu, B.; Zeng, J.; Nie, H.; Xiong, Y.; Zou, J.; Ning, H.; Wang, Z.; Zhao, Z.; Tang, B. Z. Efficient Bipolar Blue AIEgens for High-Performance Nondoped Blue OLEDs and Hybrid White OLEDs. *Adv. Funct. Mater.* **2018**, *28*, 1803369.
(21) Wang, S.; Qiao, M.; Ye, Z.; Dou, D.; Chen, M.; Peng, Y.; Shi, Y.; Yang, X.; Cui, L.; Li, J.; et al. Efficient Deep-Blue Electrofluorescence with an External Quantum Efficiency Beyond 10%. *iScience* **2018**, *9*, 532−541.
(22) Yang, Z.; Mao, Z.; Xie, Z.; Zhang, Y.; Liu, S.; Zhao, J.; Xu, J.; Chi, Z.; Aldred, M. P. Recent Advances in Organic Thermally Activated Delayed Fluorescence Materials. *Chem. Soc. Rev.* **2017**, *46*, 915−1016.
(23) Wu, C.; Wang, B.; Wang, Y.; Hu, J.; Jiang, J.; Ma, D.; Wang, Q. A Universal Host Material with a Simple Structure for Monochrome and White Phosphorescent/TADF OLEDs. *J. Mater. Chem. C* **2019**, *7*, 558−566.
(24) Cai, X.; Su, S.-J. Marching Toward Highly Efficient, Pure-Blue, and Stable Thermally Activated Delayed Fluorescent Organic Light-Emitting Diodes. *Adv. Funct. Mater.* **2018**, *28*, 1802558.
(25) Tao, Y.; Yuan, K.; Chen, T.; Xu, P.; Li, H.; Chen, R.; Zheng, C.; Zhang, L.; Huang, W. Thermally Activated Delayed Fluorescence Materials Towards the Breakthrough of Organoelectronics. *Adv. Mater.* **2014**, *26*, 7931−7958.
(26) Wei, Q.; Fei, N.; Islam, A.; Lei, T.; Hong, L.; Peng, R.; Fan, X.; Chen, L.; Gao, P.; Ge, Z. Small-Molecule Emitters with High Quantum Efficiency: Mechanisms, Structures, and Applications in OLED Devices. *Adv. Opt. Mater.* **2018**, *6*, 1800512.
(27) Wang, Z.; Li, Y.; Cai, X.; Chen, D.; Xie, G.; Liu, K.; Wu, Y.-C.; Lo, C.-C.; Lien, A.; Cao, Y.; et al. Structure−Performance Investigation of Thioxanthone Derivatives for Developing Color Tunable Highly Efficient Thermally Activated Delayed Fluorescence Emitters. *ACS Appl. Mater. Interfaces* **2016**, *8*, 8627−8636.
(28) Yao, L.; Yang, B.; Ma, Y. Progress in Next-Generation Organic Electroluminescent Materials: Material Design beyond Exciton Statistics. *Sci. China: Chem.* **2014**, *57*, 335−345.
(29) Tang, X.; Bai, Q.; Peng, Q.; Gao, Y.; Li, J.; Liu, Y.; Yao, L.; Lu, P.; Yang, B.; Ma, Y. Efficient Deep Blue Electroluminescence with an External Quantum Efficiency of 6.8% and $CIE_{<i>y</i>}$ < 0.08 Based on a Phenanthroimidazole−Sulfone Hybrid Donor−Acceptor Molecule. *Chem. Mater.* **2015**, *27*, 7050−7057.
(30) Khalid, M.; Hussain, R.; Hussain, A.; Ali, B.; Jaleel, F.; Imran, M.; Assiri, M. A.; Usman Khan, M.; Ahmed, S.; Abid, S.; et al. Electron Donor and Acceptor Influence on the Nonlinear Optical Response of Diacetylene-Functionalized Organic Materials (DFOMs): Density Functional Theory Calculations. *Molecules* **2019**, *24*, 2096.
(31) Mohan, N.; Suresh, C. H.; Kumar, A.; Gadre, S. R. Molecular Electrostatics for Probing Lone Pair−π Interactions. *Phys. Chem. Chem. Phys.* **2013**, *15*, 18401−18409.
(32) Girase, J. D.; Shahnawaz; Nagar, M. R.; Jayakumar, J.; Jou, J. H.; Vaidyanathan, S. New Deep Blue Fluorophores Based on Benzo[d]Thiazole Group as Acceptor Core: Theoretical, Synthesis, Photophysical and Electroluminescent Investigation. *J. Lumin.* **2022**, *248*, 118992.
(33) Girase, J. D.; Tagare, J.; Shahnawaz; Nagar, M. R.; Siddiqui, I.; Jou, J.-H.; Patel, S.; Vaidyanathan, S. Deep-Blue Emitters (CIEy ∼0.07) Based on Phenanthroimidazole: Remarkable Substitution Effects at the N1 Position of Imidazole on the Excited States and Electroluminescence Properties. *Dyes Pigm.* **2021**, *196*, 109791.
(34) Chen, L.; Chen, K.; Yao, R.; Zeng, R.; Lin, Y.; Jian, R.; Bai, W. From Blue Fluorescence to Red Fluorescence: Solid-State Oxidative Coupling Polymerization of Fluorene and Anthracene or Naphthalene. *Mater. Chem. Phys.* **2022**, *285*, 126083.
(35) Wang, Z.; Lu, P.; Chen, S.; Gao, Z.; Shen, F.; Zhang, W.; Xu, Y.; Kwok, H. S.; Ma, Y. Phenanthro[9,10-d]Imidazole as a New Building Block for Blue Light Emitting Materials. *J. Mater. Chem.* **2011**, *21*, 5451−5456.
(36) Lin, G.; Zhang, X.; Li, Y.; Allen, W.; Noda, I.; Mark, J. E. Some Nanocomposites Based On a Glycerol-Derived Alkyd Resin and Layered Silicates. *Mol. Cryst. Liq. Cryst.* **2008**, *483*, 33−48.
(37) de Leeuw, D. M.; Simenon, M. M. J.; Brown, A. R.; Einerhand, R. E. F. Stability of N-Type Doped Conducting Polymers and Consequences for Polymeric Microelectronic Devices. *Synth. Met.* **1997**, *87*, 53−59.
(38) Ganzorig, C.; Fujihira, M. A Possible Mechanism for Enhanced Electrofluorescence Emission through Triplet−Triplet Annihilation in Organic Electroluminescent Devices. *Appl. Phys. Lett.* **2002**, *81*, 3137−3139.
(39) Romain, M.; Quinton, C.; Roisnel, T.; Jacques, E.; Rault-Berthelot, J.; Poriel, C. A. D. A Dihydrodinaphthoheptacene. *J. Org. Chem.* **2018**, *83*, 1891−1897.
(40) Cho, I.; Kim, S. H.; Kim, J. H.; Park, S.; Park, S. Y. Highly Efficient and Stable Deep-Blue Emitting Anthracene-Derived Molecular Glass for Versatile Types of Non-Doped OLED Applications. *J. Mater. Chem.* **2012**, *22*, 123−129.
(41) Yan, Y.-N.; Pan, W.; Song, H.-C. The Synthesis and Optical Properties of Novel 1,3,4-Oxadiazole Derivatives Containing an Imidazole Unit. *Dyes Pigm.* **2010**, *86*, 249−258.
(42) Lv, H.; Wei, L.; Guo, S.; Zhang, X.; Chen, F.; Qin, X.; Wei, C.; Jiang, B.; Gong, Y. Ionic Rigid Organic Dual-State Emission Compound With Rod-Shaped and Conjugated Structure for Sensitive Al3+ Detection. *Front. Chem.* **2022**, *10*, 807088.
(43) Zhou, G.; Wong, W.-Y.; Suo, S. Recent Progress and Current Challenges in Phosphorescent White Organic Light-Emitting Diodes (WOLEDs). *J. Photochem. Photobiol., C* **2010**, *11*, 133−156.
(44) Wang, J.; Dang, Q.; Gong, Y.; Liao, Q.; Song, G.; Li, Q.; Li, Z. Precise Regulation of Distance between Associated Pyrene Units and Control of Emission Energy and Kinetics in Solid State. *CCS Chem.* **2021**, *3*, 274−286.
(45) Sauer, M.; Hofkens, J.; Enderlein, J. *Handbook of Fluorescence Spectroscopy and Imaging: From Ensemble to Single Molecules*; Wiley, 2010.
(46) Xu, A.; Wang, G.; Li, Y.; Dong, H.; Yang, S.; He, P.; Ding, G. Carbon-Based Quantum Dots with Solid-State Photoluminescent: Mechanism, Implementation, and Application. *Small* **2020**, *16*, 2004621.
(47) Yang, G.-X.; Chen, Y.; Zhu, J.-J.; Song, J.-Y.; Tang, S.-S.; Ma, D.; Tong, Q.-X. Rational Design of Pyridine-Containing Emissive Materials for High Performance Deep-Blue Organic Light-Emitting Diodes with CIEy ∼ 0.06. *Dyes Pigm.* **2021**, *187*, 109088.
(48) Jayabharathi, J.; Thilagavathy, S.; Thanikachalam, V. Blue Organic Light-Emitting Diodes with Hybridized Local and Charge-Transfer Excited State Realizing High External Quantum Efficiency. *RSC Adv.* **2021**, *11*, 8606−8618.

(49) Grabowski, Z. R.; Rotkiewicz, K.; Rettig, W. Structural Changes Accompanying Intramolecular Electron Transfer: Focus on Twisted Intramolecular Charge-Transfer States and Structures. *Chem. Rev.* **2003**, *103*, 3899−4032.
(50) Li, W.; Pan, Y.; Yao, L.; Liu, H.; Zhang, S.; Wang, C.; Shen, F.; Lu, P.; Yang, B.; Ma, Y. A Hybridized Local and Charge-Transfer Excited State for Highly Efficient Fluorescent OLEDs: Molecular Design, Spectral Character, and Full Exciton Utilization. *Adv. Opt. Mater.* **2014**, *2*, 892−901.
(51) Zhu, Z.-L.; Ni, S.-F.; Chen, W.-C.; Yuan, Y.; Tong, Q.-X.; Wong, F.-L.; Lu, F.; Lee, C.-S. A High Performance Deep-Blue Emitter with an Anti-Parallel Dipole Design. *Dyes Pigm.* **2017**, *146*, 219−225.
(52) Lippert, E. Spektroskopische Bestimmung Des Dipolmomentes Aromatischer Verbindungen Im Ersten Angeregten Singulettzustand. *Z. Elektrochem., Ber. Bunsenges. Phys. Chem.* **1957**, *61*, 962−975.
(53) Mataga, N.; Kaifu, Y.; Koizumi, M. Solvent Effects upon Fluorescence Spectra and the Dipolemoments of Excited Molecules. *Bull. Chem. Soc. Jpn.* **1956**, *29*, 465−470.
(54) Jayabharathi, J.; Anudeebhana, J.; Thanikachalam, V.; Sivaraj, S. Efficient Fluorescent OLEDS Based on Assistant Acceptor Modulated HLCT Emissive State for Enhancing Singlet Exciton Utilization. *RSC Adv.* **2020**, *10*, 8866−8879.
(55) Tagare, J.; Ulla, H.; Satyanarayan, M. N.; Vaidyanathan, S. Efficient Non-Doped Bluish-Green Organic Light Emitting Devices Based on N1 Functionalized Star-Shaped Phenanthroimidazole Fluorophores. *J. Photochem. Photobiol., A* **2018**, *353*, 53−64.
(56) Usta, H.; Alimli, D.; Ozdemir, R.; Tekin, E.; Alkan, F.; Kacar, R.; Altas, A. G.; Dabak, S.; Gürek, A. G.; Mutlugun, E.; et al. A Hybridized Local and Charge Transfer Excited State for Solution-Processed Non-Doped Green Electroluminescence Based on Oligo(p-Phenyleneethynylene). *J. Mater. Chem. C* **2020**, *8*, 8047−8060.

https://doi.org/10.1021/acs.jpcc.3c00790
J. Phys. Chem. C 2023, 127, 10291−10302